Journal of Nuclear Medicine, published on June 30, 2022 as doi:10.2967/jnumed.122.264152

^{18}F-Fluciclovine PET Imaging of Glutaminase Inhibition in Breast Cancer Models

Rong Zhou, PhD[1]*, Hoon Choi, PhD[1], Jianbo Cao, PhD[1], Austin Pantel, MD[1], Mamta Gupta, PhD[1], Hsiaoju S. Lee, PhD[1], David Mankoff, MD, PhD[1]*

[1]Department of Radiology, University of Pennsylvania, Philadelphia, PA

Financial support:

This study was supported by R21CA198563, R01CA211337 and Komen SAC130060. ^{18}F-Fluciclovine and CB839 were generously provided by Blue Earth Diagnostics and Calithera, respectively.

***Authors responsible for correspondence:**

Rong Zhou, PhD
Research Professor
Department of Radiology
University of Pennsylvania
John Morgan 198
3620 Hamilton Walk
Philadelphia, PA 19104
Phone: 215-746-8787
Fax: 215-573-2255
rongzhou@pennmedicine.upenn.edu

David Mankoff, MD, PhD, Professor
Division of Nuclear Medicine
Department of Radiology
University of Pennsylvania
116 Donner, HUP
3400 Spruce Street
Philadelphia, PA 19104
Phone: 215-615-3687
Fax : 215-349-5843
david.mankoff@pennmedicine.upenn.edu

Total # words: 4995

Running title

^{18}F-Fluciclovine as a marker of GLSi

ABSTRACT

Aggressive cancers such as triple-negative breast cancer (TNBC) avidly metabolize glutamine as a feature of their malignant phenotype. The conversion of glutamine to glutamate by the glutaminase (GLS) enzyme represents the first and rate-limiting step of this pathway, and a target for drug development. Indeed, a novel GLS inhibitor (GLSi) has been developed and tested in clinical trials, but with limited success, suggesting the potential for a biomarker to select patients that could benefit from this novel therapy. Here, we study a non-metabolized amino acid analog, ^{18}F-Fluciclovine (Axumin®) as a PET imaging biomarker for detecting the pharmacodynamic response to GLSi. We show that glutamine transporters mediate the uptake of ^{18}F-Fluciclovine into human breast cancer cells. To allow ^{18}F-Fluciclovine PET to be performed in mice, citrate in the tracer formulation is replaced by PBS. Mice bearing TNBC (HCC38, HCC1806 and MBA-MD-231) and ER-positive (MCF-7) breast cancer xenografts were imaged with dynamic PET at baseline and after a 2-day treatment of GLSi (CB839 (Telaglenastat)) or vehicle. Kinetic analysis suggested reversible uptake of the tracer and the distribution volume (V_D) of ^{18}F-Fluciclovine was estimated by Logan plot analysis. A significant increase of V_D was observed after CB839 treatment in TNBC models exhibiting high GLS activity (HCC38 and HCC1806), but not in TNBC or MCF-7 exhibiting low GLS. Changes of V_D were corroborated with changes in GLS activity measured in CB839- *versus* vehicle-treated tumors, as well as with changes of V_D of [^{18}F]-(2S,R4)-fluoroglutamine, which we previously validated as a measure of cellular glutamine pool size. A moderate, albeit significant decrease of [^{18}F]fluorodeoxyglucose (FDG) PET signal was observed in HCC1806 tumors after CB839 treatment. In conclusion, ^{18}F-Fluciclovine PET has potential to serve as a clinical translatable, pharmacodynamic biomarker of GLSi.

KEY WORDS

^{18}F-Fluciclovine PET, Triple negative breast cancer, Glutaminase, Distribution volume, CB839

INTRODUCTION

Reprogramming of energy metabolism has been recognized as a hallmark of cancer (1). Dysregulation of cellular metabolic pathways enables cancer cells to meet their energetic and biosynthetic needs, but also provides opportunities to selectively target cancer cells while sparing normal tissues. Targeting such a cancer-specific metabolic signature could be useful for treating triple-negative breast cancers (TNBC), which lacks a subtype-specific treatment due to absence of the estrogen receptor (ER), the progesterone receptor (PR), and the human epidermal growth factor receptor 2. Glutaminolysis, the metabolic pathway of glutamine, is utilized by many aggressive cancers, including TNBC (2,3) hence could be exploited for therapy. Conversion of glutamine to glutamate by the mitochondrial enzyme glutaminase (GLS) represents the first and rate-limiting step in the pathway. In cancers, it is the kidney type rather than liver type GLS is predominantly expressed. Highly potent and specific inhibitors of GLS (GLSi) have been developed. Several of these agents have shown promise in pre-clinical studies (4-7) and one agent, CB839 (Telaglenastat®), has advanced into clinical trials. While CB839 has been well tolerated in clinical trials, efficacy has been variable (8-10). These trials, though, did not include biomarkers to assess target impact to guide patient selection, potentially confounding the overall study results. While enhanced glutamine metabolism is frequently observed in TNBC, more so than other subtypes of breast cancer, individual TNBCs are highly heterogenous and exhibit a wide range of GLS activity (4). As such, a method to evaluate the pharmacodynamic response of TNBC to GLSi would be highly valuable for patient selection in the clinical setting where GLS activity cannot be readily assessed.

Previous studies have elucidated an inverse relationship between GLS activity and glutamine pool size, providing a paradigm for imaging glutamine metabolism with amino acids analogs. Tumors

with a high GLS activity have low cellular glutamine concentration (pool size) accompanied by a high glutamate (the product of the GLS) level (4). Upon GLS inhibition, the cellular glutamine pool increases due to blockade of glutamine conversion to glutamate (4,11). It follows that such an increase in tumor cellular glutamine pool size can serve as a specific pharmacodynamic (PD) marker for GLSi.

Our approach to measure the change in tumor pool glutamine size relies on tracers that mimic bi-directional glutamine transport in/out of the cancer cell but are not metabolized by *GLS*. Under these conditions, and assuming stable kinetics for glutamine transport and metabolism over the course of the imaging study (~1 hour), the tracer will fit a single reversible tracer kinetic model (12), where the distribution volume fraction (V_D) provides a direct measure of intracellular glutamine concentration. We and others have previously shown that cellular uptake of the amino acid analog, [^{18}F]-(2S,4R)4-Fluoroglutamine (^{18}F-4F-Gln) matches the native glutamine transporters (13) but is a poor substrate for kidney-type GLS expressed in the tumor (14,15). Furthermore, in human breast cancer xenograft models, V_D of ^{18}F-4F-Gln PET or the tumor-to-blood ratio (T/B) 30 minutes or later after injection can serve serves as PD marker of GLSi (15,16).

^{18}F-4F-Gln, however, is an investigational agent, has been reported to undergo defluorination (17,18), which could confound the PET signal and potentially mask bone disease, a common site of breast cancer metastasis. To overcome these limitations, we considered ^{18}F-Fluciclovine (Axumin®), a metabolically inert analogue of L-leucine (16) and uptake into cancer cells mediated by glutamine transporters (19,20). Hence, ^{18}F-Fluciclovine may serve as an alternative tracer for measuring glutamine pool size and the impact of GLSi. While ^{18}F-Fluciclovine has been studied under investigational settings for breast cancer (21,22), its utility as a metabolic marker has not been established. Herein, we performed a proof-of-principle study of ^{18}F-Fluciclovine as a

pharmacodynamic marker for GLSi, comparing with ^{18}F-4F-Gln by applying the same tumor models and analysis methods (15,16). We were able to show that (i) the uptake of ^{18}F-Fluciclovine is mediated by glutamine transporters; (ii) ^{18}F-Fluciclovine has reversible kinetics that reflects cellular glutamine pool size, and (iii) short-term exposure to GLSi demonstrates changes in ^{18}F-Fluciclovine V_D like ^{18}F-4F-Gln.

MATERIALS AND METHODS

Materials

^{18}F-Fluciclovine was provided by Blue Earth Diagnostics (Burlington, MA). Vehicle solution (VEH) of 25% (w/v) hydroxypropyl-β-cyclodextrin in 10 mmol/L citrate (pH 2)(15) and CB839 (Telaglenastat®) dissolved in VEH or in DMSO were provided by Calithera Biosciences (Palo Alto, CA). [^{18}F](2S,4R)4-fluoroglutamine (15) and [^{18}F]FDG were produced at the PET Center, University of Pennsylvania.

The following reagents, assay kits, and cell lines were purchased: ion-exchange resins columns (Catalog number: 731621 from Bio-Rad (Hercules, CA); Citrate Assay Kit (Catalog number: MAK057), *L*-Glutamine (Gln), GPNA (L-γ-Glutamyl-p-nitroanilide) and BCH (2-aminobicyclo-(2,2,1)-heptane-2-carboxylic acid) all from Sigma (St. Louis, MO); Syringe filter (Catalog number: 09-720-3) and 96-well strip plate (catalog number: 07-200-97) from Fisher Scientific (Pittsburgh, PA); human TNBC (HCC1806, HCC38, MDA-MB-231) and ER+ (MCF-7) breast cancer cell lines from ATCC (Manassas, VA). The cell lines were authenticated using the Short Tandem Repeat DNA profiling method and were used within six months from the date of purchase.

Cells were maintained in complete culture media consisting of RPMI-1640 (catalog #: 25-506, GenClone) supplemented with 10% HyClone FBS without antibiotics.

Removal of citrate from the formulation of ^{18}F-Fluciclovine

Following releasing the de-ionized water from the column resin, the column was loaded with the tracer solution (~ 0.9 mL) provided by the vendor. An equal volume (0.9 mL) of PBS was added to the column and the eluded solution was collected (~0.9 mL in 1~2 min) in a sterile test tube (Tube-1). This was repeated by adding PBS (0.9 mL) and collecting the elution in Tube-2. The [^{18}F] activity in the eluted solution was estimated by a dose calibrator (Capintec, CRC-7, Florham Park, NJ) while the pH and residual citrate in the solution were assessed by pH test strips and citrate assay, respectively.

***In vitro* cell uptake of ^{18}F-Fluciclovine**

Breast cancer lines HCC38, HCC1806, and MCF-7 were included. Cells (30, 25 and 30k cells/well for HCC38, HCC1806, and MCF-7, respectively) were seeded in a 96-well strip plate and incubated overnight in complete culture media. To study tracer uptake, cells were incubated in PBS containing 5 mM glucose and 100 µM Gln to which ^{18}F-Fluciclovine (~300,000 cpm/well) was added at time zero. To test whether Fluciclovine uptake is mediated by Gln transporters, Gln (5 mM), GPNA (1 mM), BCH (10 mM), or DMSO control (0.05%) in PBS containing 5 mM glucose was added at time zero. After a specified incubation time (5, 15, 30, 60 and 120 min), supernatant was aspirated, and the wells were washed twice with cold PBS. After washing, activity in each well was counted on a gamma counter (2470 WIZARD2, Perkin Elmer, Waltham, MA), the amount of protein was estimated by Lowry method (15). To inhibit *GLS* activity, the cells were incubated in culture media containing 1 µM CB839 or 0.05% DMSO as control for 24 h before

cell uptake studies because cellular metabolites concentration remain unchanged during 24 h of incubation with CB839 (4); the drug was present during incubation with the radiotracer.

Human breast cancer xenograft models and treatment with GLSi (CB839)

All animal procedures were approved by the institutional animal care and usage committee (IACUC) of the University of Pennsylvania. NCR athymic nu/nu mice (female, 7-week-old) were purchased from Charles River. To establish the human breast cancer xenografts, $1x10^6$ HCC1806 cells in 100 µL PBS, $5x10^6$ MCF-7 or HCC38 cells in 150 µL Matrigel solution (1: 1 mixed with PBS) were subcutaneously inoculated into the right flank of the mouse. Tumor size was measured by a reader who was blinded to PET image analysis using a caliper in two orthogonal directions (a and b with b being the shorter dimension) using formula: $V= (1/6)*\pi*a*b^2$. CB839, dissolved in the vehicle solution (VEH) (15) was administered via oral gavage (200 mg/kg twice daily) for 2 days; control mice received the same volume of VEH solution (~0.25 mL).

Quantification of GLS activity in cells and tumor tissues

To process cells for GLS activity, a pellet of 10 million cells was suspended in 1mL of homogenization buffer (50 mM Tris-Acetate pH 8.6, 15 mM K_2HPO_4, 150 mM KCl, 0.25 mM EDTA, 1 mM DTT including 1x complete protease inhibitor) in a 2 mL tube containing ceramic beads (Bertin Instruments, Rockville, MD). Tumor tissue was clamp-frozen in liquid nitrogen upon euthanasia of the mouse and kept in -80°C freezer. The homogenization buffer (as above) was added to the weighed tissue (v/w = 10/1) in a 2 mL tube containing ceramic beads.

Homogenization of cell or tissue samples was performed at 4°C using a PRECELLYS® Evolution homogenizer equipped with CRYOLYS® Evolution (Bertin Instruments). The supernatant was removed and passed through a gel filtration spin column (Zeba Spin Desalting Column, Fisher

Scientific). The filtered supernatant and substrates, including glutamate dehydrogenase, NADP+, and glutamine, were mixed to start the enzymatic reaction generating NADPH which was detected by fluorescence (Ex340/ Em460) and recorded every minute for 15 min at 25°C in a Microplate Reader (SpectraMax M5, Molecular Devices). Specific activity was calculated from the background corrected velocity (nmol NADPH/min) divided by the amount of protein. A standard curve was produced using pure glutaminase (Catalog number: G8880, Sigma) .

***In vivo* PET/CT imaging and analysis of dynamic PET images**

In vivo PET/CT was performed on the Molecubes modular system (Molecubes Corporation, Ghent, Belgium) before and after treatment. 200~250 μCi of ^{18}F-Fluciclovine in 0.2 mL was injected into the tail vein catheter and a 45-min dynamic PET scan was started immediately and followed by a 2 min CT scan. The dynamic PET data were reconstructed with a temporal resolution of 10 sec/frame x 6, 1 min/frame x 9, and 5 min/frame x 7 frames. FDG PET imaging was applied to a separate cohort of mice subjected to the same treatment. After 4 h fasting, the mouse was injected with 100 μCi FDG and recovered from anesthesia. Two hours after FDG injection, the mouse was anesthetized and underwent 15-min static PET scan.

PET data were analyzed using PMOD software version 3.711 (Zürich, Switzerland). A spherical ROI equal to 1/8 volume of the tumor size (measured by caliber before imaging) was placed over the hottest region of the tumor while avoiding activities from nearby bones by referencing to the CT image. Time activity curve (TAC) of the tumor was then obtained from the respective ROI. To measure the activity in the blood, a 2×2×2 mm^3 cube ROI was placed over the left ventricle heart of the mouse by referencing to the CT image. The image analysis methods used in this study match to those of ^{18}F-4F-Gln (15,16), including the tumor ROI size. TAC of the blood and tumor were imported to the General Kinetic Modeling Tool (PKIN) of PMOD for analyses. Based on

preliminary analyses, the kinetic data fit both a 1- and 2-compartment model, but the 2-compartment model fit returned a small k_3 value (0-0.02/min), consistent with a reversible uptake of the tracer as reported earlier for ^{18}F-4F-Gln in mice (16) and patients (23). Henceforward, given reversible uptake, Logan plot (24), a simplified graphical method based on compartment model analysis, was used to estimate tracer distribution volume fraction (V_D) of the tumor.

Statistical Analysis

Data are presented as mean +/- SD (error bars). Statistical tests were performed using GraphPad Prism 6 (San Diego, CA). Two-sided student *t*-test was used to evaluate difference between two groups with α set at 0.05.

RESULTS

Citrate assay results demonstrated that the column filtration protocol almost completely removed citrate while >80% of ^{18}F radioactivity was recovered in eluted PBS with activity concentration of 4.6 - 5 mCi/ml suitable for injection into mice (Supplemental Figure 1A-B). The citrate-replaced tracer solution appeared safe without causing weight loss over 7 days (Supplemental Figure 1C).

To assess whether ^{18}F-Fluciclovine uptake is mediated by glutamine transporters, tracer uptake was measured in the presence and absence of cold glutamine and pharmacological inhibitors of ASCT2 and LAT (Figure 1). ^{18}F-Fluciclovine uptake was blocked ~100%, 82% and 56% by cold glutamine, BCH and GPNA, respectively at 30 min compared to the control (P <0.00001 for all).

We then evaluated the impact of *GLS*i on ^{18}F-Fluciclovine uptake in human TNBC (HCC38 and HCC1806) and an ER+ BC (MCF-7) cells, which exhibit distinct *GLS* activity (HCC38>

HCC1806 >> MCF-7). Consistent with reversible uptake pattern, the uptake peaked around 30 min followed by washout shown in Figure 2A-C: at 30 min, tracer uptake was significantly higher in CB839-treated HCC38 and HCC1806 cells compared to vehicle controls, but such difference was minimal in MCF-7 cells. Corroborated by GLS activities in the presence and absence of GLSi (Figure 2D), these data suggest that inhibition of active GLS results in a large increase in glutamine pool size that is reflected in significant increases of ^{18}F-Fluciclovine uptake in these cells.

Logan plots of PET data acquired before treatment revealed distinct slope (V_D) of the three models (HCC38 < HCC1806 < MCF-7, Supplemental Figure 2A), inverse to their GLS activity. *In vivo* static PET images (last frame) revealed an increase of ^{18}F-Fluciclovine PET signal in HCC38 and HCC1806 tumor after GLSi treatment (Supplemental Figure 2B). Changes in V_D were then examined: In the HCC1806 model, a significant increase in V_D was observed after a short course (2 days) of CB839 treatment (pre *versus* post of 1.24 ± 0.26 vs. 2.05 ± 0.26, $P = 0.0055$, paired *t*-test, n = 6, Figure 3A); For comparison, V_D of the VEH control group showed a non-significant decrease (pre *versus* post V_D of 1.33 ± 0.24 vs. 1.05 ± 0.20, $P = 0.24$, paired *t*-test, n=7). Changes of T/B shown in Supplemental Figure 3 are consistent with changes in V_D. Two additional TNBC models were examined in fewer number of mice: V_D was increased by an average of 23% after CB839 (n = 3) compared to 37% decrease post VEH treatment (n = 2) in HCC38 tumors (high GLS); V_D was decreased by 5% and 7% after CB839 treatment (n =1) and VEH treatment (n = 2), respectively in MDA-MB-231 tumors (low GLS activity).

We further compared V_D of ^{18}F-Fluciclovine *versus* V_D of ^{18}F-4F-Gln PET (Figure 4): In HCC1806 model, a large increase of V_D (slope of logan plot) was observed in both ^{18}F-Fluciclovine and ^{18}F-4F-Gln after CB839 treatment compared to baseline (Figure 4A-B); in MCF-7, only a modest change of the slope was detected (Figure 4C-D). In some mice, an overall increase

of [^{18}F] PET signal was observed after CB839 treatment, likely due to an increase in plasma glutamine level after CB839 exposure (15), leading to decreased clearance of ^{18}F-4F-Gln or ^{18}F-Fluciclovine. Groupwise, CB839 treatment led to an increase in V_D (89 ± 39%) compared to a decrease (-16 ± 11%) after VEH treatment in HCC1806 model (Figure 3B, P <0.05); modest changes were observed in MCF-7 tumors after CB839 or VEH treatment (P =0.6). These values compare favorably to ^{18}F-4F-Gln PET: T/B estimated directly from PET images acquired from 30-45 min is a proxy of V_D and was increased by 34 ±14% in HCC1806 tumors post CB839 compared to -11 ± 24% after VEH treatment (15), and T/B and V_D was highly correlated (r^2 = 0.92) (16). GLS enzymatic activity measured from tumor tissues revealed a large, 3-fold reduction in HCC1806 tumors post CB839 treatment compared to VEH controls, whereas no significant change in MCF-7 tumors (Figure 3C).

Finally, we tested whether FDG PET can detect responses to CB839 treatment (Supplemental Figure 4A-B). A moderate albeit significant decrease of FDG PET signal (%ID/g) was observed in HCC1806 tumors after CB839 treatment (pre vs. post: 2.94 ± 0.24 vs. 2.29 ± 0.21, n = 11, P < 0.05); a decrease was also observed in VEH group, but it is not significant (pre vs. post: 3.47 ± 0.59 vs. 2.47 ± 0.016, n = 5, P = 0.31).

DISCUSSION

Blockade of ^{18}F-Fluciclovine cell uptake by glutamine, as well as by pharmacological inhibitor of LAT (BCH) and ASCT2 (GPNA), respectively confirms that that ^{18}F-Fluciclovine enters the cells via glutamine transporters. Indeed, prior studies have shown that ASCT2 transporter mediates glutamine uptake in many cancer cells (13,25) including TNBC (26). In vivo PET studies

demonstrate a large increase of V_D in TNBC models exhibiting high GLS activity (HCC1806 and HCC38) after a short course of GLSi treatment. However, no increase was detected after VEH (control) treatment or in models exhibiting low GLS activity (MD-MBA-231 and MCF-7). These results are corroborated by GLS activities in tumor specimens and support that increased ^{18}F-Fluciclovine uptake reflects inhibition of active GLS. The ability of ^{18}F-Fluciclovine to report pharmacodynamic response to GLSi enables early detection of target engagement and predicting GLSi futility if the tumor fails to demonstrate an alteration in tracer uptake kinetics in response to the drug. This approach using a target-specific drug with short-term exposure as a perturbogen, and a mechanistically matched tracer, has been tested in other scenarios, including human studies of drug efflux inhibitors (27), estrogen receptor agonists (28), and estrogen receptor blockade (29). It is possible, and likely, that longer exposure may lead to differences in results, as was seen in studies where residual ^{18}F-Fluciclovine was tested as a marker of resistant, viable tumor (22). The time course of the increase in tumor glutamine pool size and matched alteration in ^{18}F-Fluciclovine kinetics will need to be studied in future pre-clinical and clinical studies testing ^{18}F-Fluciclovine as a marker to guide GLS-targeted therapy.

Our data also revealed that FDG PET is not a sensitive marker for GLSi likely because glucose uptake or metabolism is not directly impacted by short exposure to GLSi (4). FDG can likely serve as a marker of cell viability or death over extended periods of time, as it does for a variety of cancer cell types and treatments (30).

The approach of utilizing amino acid analogs that are not metabolized nor substrates for biosynthesis differs fundamentally from that of metabolized tracers such as [^{11}C]Glutamine (31), which participates in biosynthesis and metabolized through glutaminolysis to produce [^{11}C]CO_2 and radiolabeled metabolites (e.g., [^{11}C]Glutamate), leading to a complex distribution of the

radiolabel which must be accounted for. While [^{11}C]Glutamine has been recently been studied in human subjects (32), the complexity behind the C-11 PET signal would be a challenge for proper interpretation of PET signal changes and widespread clinical adoption. In contrast, complexity is mitigated with non-metabolized tracers, such as ^{18}F-Fluciclovine whereby enzymatic activity and drug effect is inferred from changes in pool size (33,34). The favorable comparison of the V_D of ^{18}F-Fluciclovine *versus* ^{18}F-4F-Gln (Figure 4) strongly suggests that clinical translation could be facilitated by ^{18}F-Fluciclovine due to its superior chemical stability, widespread consensus regarding lack of metabolism (35) and commercial availability.

Our study has a few limitations. First, while changes of V_D observed in two other TNBC models (HCC38 and MDA-MB-231) were consistent with the expectation, their sample sizes were relatively small. However, a primary goal of this study was to compare V_D of ^{18}F-Fluciclovine with V_D of ^{18}F-4F-Gln previously estimated in HCC1806 and MCF-7 models (15,16). Second, tumor glutamine pool sizes were not directly quantified; in previous study however, glutamine concentration was measured independently by 1H NMR technique in HCC1806 and MCF-7 tumors after the same treatment regimen and a strong correlation was found between tumor glutamine pool size *versus* T/B, a proxy of V_D (15).

The findings of the current study suggest that ^{18}F-Fluciclovine PET provides a tool for assessing tumor glutamine pool size and can serve as a PD marker for *GLS*i (such as CB839). The favorable biochemical properties and established availability of this tracer make it an attractive candidate for future human translation.

FINANCIAL DISCLOSURES

This study was supported by R21CA198563, R01CA211337 and Komen SAC130060. ^{18}F-Fluciclovine and CB839 were generously provided by Blue Earth Diagnostics and Calithera, respectively. No potential conflicts of interest relevant to this article exist.

ACKNOWLEDGEMENT

^{18}F-Fluciclovine and CB839 were generously provided by Blue Earth Diagnostics and Calithera, respectively. We are grateful to Dr. Varsha Viswanath and Daniel Kranseler for assistance in data processing and to Drs. Karen Linder and Hamed Hossein of Blue Earth Diagnostics for insightful discussions. This study was supported by R21CA198563, R01CA211337 and Komen SAC130060.

KEY POINTS

Question: Can ^{18}F-Fluciclovine PET report the pharmacodynamic effect of glutaminase inhibitor in glutaminase active breast cancers?

Pertinent findings: ^{18}F-Fluciclovine is taken up in breast cancer cells via glutamine transporters and is not metabolized thus ^{18}F-Fluciclovine is capable of tracking glutamine pool size. In human breast cancer models of differential glutaminase activity, a significant increase of ^{18}F-Fluciclovine VD was observed after glutaminase inhibitor (CB839) treatment in tumor models exhibiting high GLS activity, but not in those with low activity.

Implications for patient care: ^{18}F-Fluciclovine PET marker might provide information that can help select patients for treatment targeting glutamine metabolism such as glutaminase inhibitors.

REFERENCES

1. Hanahan D, Weinberg RA. Hallmarks of cancer: the next generation. Cell 2011;144(5):646-74.
2. DeBerardinis RJ, Cheng T. Q's next: the diverse functions of glutamine in metabolism, cell biology and cancer. Oncogene 2010;29(3):313-24.
3. DeBerardinis RJ, Lum JJ, Hatzivassiliou G, Thompson CB. The biology of cancer: metabolic reprogramming fuels cell growth and proliferation. Cell Metab 2008;7(1):11-20.
4. Gross MI, Demo SD, Dennison JB, Chen L, Chernov-Rogan T, Goyal B, et al. Antitumor activity of the glutaminase inhibitor CB-839 in triple-negative breast cancer. Mol Cancer Ther 2014;13(4):890-901.
5. Boysen G, Jamshidi-Parsian A, Davis MA, Siegel ER, Simecka CM, Kore RA, et al. Glutaminase inhibitor CB-839 increases radiation sensitivity of lung tumor cells and human lung tumor xenografts in mice. International Journal of Radiation Biology 2019;95(4):436-42.
6. Momcilovic M, Bailey ST, Lee JT, Fishbein MC, Magyar C, Braas D, et al. Targeted Inhibition of EGFR and Glutaminase Induces Metabolic Crisis in EGFR Mutant Lung Cancer. Cell reports 2017;18(3):601-10.
7. Hoerner CR, Chen VJ, Fan AC. The 'Achilles Heel' of Metabolism in Renal Cell Carcinoma: Glutaminase Inhibition as a Rational Treatment Strategy. Kidney Cancer. Volume 32019. p 15-29.
8. Meric-Bernstam F, Tannir NM, Mier JW, DeMichele A, Telli ML, Fan AC, et al. Phase 1 study of CB-839, a small molecule inhibitor of glutaminase (GLS), alone and in

combination with everolimus (E) in patients (pts) with renal cell cancer (RCC). Journal of Clinical Oncology 2016;34(15_suppl):4568-68.

9. Zhao Y, Feng X, Chen Y, Selfridge JE, Gorityala S, Du Z, et al. 5-Fluorouracil Enhances the Antitumor Activity of the Glutaminase Inhibitor CB-839 against PIK3CA-Mutant Colorectal Cancers. Cancer Res 2020;80(21):4815-27.
10. Wang Z, Liu F, Fan N, Zhou C, Li D, Macvicar T, et al. Targeting Glutaminolysis: New Perspectives to Understand Cancer Development and Novel Strategies for Potential Target Therapies. Frontiers in oncology 2020;10(2321).
11. Kung HN, Marks JR, Chi JT. Glutamine synthetase is a genetic determinant of cell type-specific glutamine independence in breast epithelia. PLoS genetics 2011;7(8):e1002229.
12. Pantel AR, Viswanath V, Muzi M, Doot RK, Mankoff DA. Principles of Tracer Kinetic Analysis in Oncology, Part II: Examples and Future Directions. J Nucl Med 2022;63(4):514-21.
13. Venneti S, Dunphy MP, Zhang H, Pitter KL, Zanzonico P, Campos C, et al. Glutamine-based PET imaging facilitates enhanced metabolic evaluation of gliomas in vivo. Science Translational Medicine 2015;7(274):274ra17.
14. Jeitner TM, Kristoferson E, Azcona JA, Pinto JT, Stalnecker C, Erickson JW, et al. Fluorination at the 4 position alters the substrate behavior of L-glutamine and L-glutamate: Implications for positron emission tomography of neoplasias. Journal of fluorine chemistry 2016;192(A):58-67.
15. Zhou R, Pantel AR, Li S, Lieberman BP, Ploessl K, Choi H, et al. [(18)F](2S,4R)4-Fluoroglutamine PET Detects Glutamine Pool Size Changes in Triple-Negative Breast Cancer in Response to Glutaminase Inhibition. Cancer Res 2017;77(6):1476-84.

16. Viswanath V, Zhou R, Lee H, Li S, Cragin A, Doot RK, et al. Kinetic Modeling of (18)F-(2S,4R)4-Fluoroglutamine in Mouse Models of Breast Cancer to Estimate Glutamine Pool Size as an Indicator of Tumor Glutamine Metabolism. J Nucl Med 2021;62(8):1154-62.
17. Ploessl K, Wang L, Lieberman BP, Qu W, Kung HF. Comparative evaluation of 18F-Labeled glutamic acid and glutamine as tumor metabolic imaging agents. Journal of Nuclear Medicine 2012;53(10):1616-24.
18. Dunphy MPS, Harding JJ, Venneti S, Zhang H, Burnazi EM, Bromberg J, et al. In Vivo PET Assay of Tumor Glutamine Flux and Metabolism: In-Human Trial of (18)F-(2S,4R)-4-Fluoroglutamine. Radiology 2018;287(2):667-75.
19. Okudaira H, Nakanishi T, Oka S, Kobayashi M, Tamagami H, Schuster DM, et al. Kinetic analyses of trans-1-amino-3-[18F]fluorocyclobutanecarboxylic acid transport in Xenopus laevis oocytes expressing human ASCT2 and SNAT2. Nuclear Medicine and Biology 2013;40(5):670-75.
20. Savir-Baruch B, Zanoni L, Schuster DM. Imaging of Prostate Cancer Using Fluciclovine. PET Clinics 2017;12(2):145-57.
21. Tade FI, Cohen MA, Styblo TM, Odewole OA, Holbrook AI, Newell MS, et al. Anti-3-¹⁸F-FACBC (¹⁸F-Fluciclovine) PET/CT of Breast Cancer: An Exploratory Study. Journal of Nuclear Medicine 2016;57(9):1357-63.
22. Ulaner GA, Goldman DA, Corben A, Lyashchenko SK, Gönen M, Lewis JS, et al. Prospective Clinical Trial of 18F-Fluciclovine PET/CT for Determining the Response to Neoadjuvant Therapy in Invasive Ductal and Invasive Lobular Breast Cancers. Journal of Nuclear Medicine 2017;58(7):1037-42.

23. Scott NP, Teoh EJ, Flight H, Jones BE, Niederer J, Mustata L, et al. Characterising 18F-fluciclovine uptake in breast cancer through the use of dynamic PET/CT imaging. British Journal of Cancer 2022;126(4):598-605.

24. Logan J, Fowler JS, Volkow ND, Wolf AP, Dewey SL, Schlyer DJ, et al. Graphical Analysis of Reversible Radioligand Binding from Time—Activity Measurements Applied to [N-11C-Methyl]-(−)-Cocaine PET Studies in Human Subjects. Journal of Cerebral Blood Flow & Metabolism 1990;10(5):740-47.

25. Schulte ML, Fu A, Zhao P, Li J, Geng L, Smith ST, et al. Pharmacological blockade of ASCT2-dependent glutamine transport leads to antitumor efficacy in preclinical models. Nat Med 2018;24(2):194-202.

26. van Geldermalsen M, Wang Q, Nagarajah R, Marshall AD, Thoeng A, Gao D, et al. ASCT2/SLC1A5 controls glutamine uptake and tumour growth in triple-negative basal-like breast cancer. Oncogene 2016;35(24):3201-8.

27. Sasongko L, Link JM, Muzi M, Mankoff DA, Yang X, Collier AC, et al. Imaging P-glycoprotein transport activity at the human blood-brain barrier with positron emission tomography. Clinical pharmacology and therapeutics 2005;77(6):503-14.

28. Dehdashti F, Wu N, Ma CX, Naughton MJ, Katzenellenbogen JA, Siegel BA. Association of PET-based estradiol-challenge test for breast cancer progesterone receptors with response to endocrine therapy. Nature communications 2021;12(1):733.

29. Wang Y, Ayres KL, Goldman DA, Dickler MN, Bardia A, Mayer IA, et al. (18)F-Fluoroestradiol PET/CT Measurement of Estrogen Receptor Suppression during a Phase I Trial of the Novel Estrogen Receptor-Targeted Therapeutic GDC-0810: Using an Imaging

Biomarker to Guide Drug Dosage in Subsequent Trials. Clin Cancer Res 2017;23(12):3053-60.

30. Mankoff DA, Eary JF, Link JM, Muzi M, Rajendran JG, Spence AM, et al. Tumor-specific positron emission tomography imaging in patients: [18F] fluorodeoxyglucose and beyond. Clin Cancer Res 2007;13(12):3460-9.

31. Qu W, Oya S, Lieberman BP, Ploessl K, Wang L, Wise DR, et al. Preparation and Characterization of l-[5-11C]-Glutamine for Metabolic Imaging of Tumors. Journal of Nuclear Medicine 2012;53(1):98-105.

32. Cohen AS, Grudzinski J, Smith GT, Peterson TE, Whisenant JG, Hickman TL, et al. First-in-human PET imaging and estimated radiation dosimetry of L-[5-¹¹C]-glutamine in patients with metastatic colorectal cancer. Journal of Nuclear Medicine 2021:jnumed.120.261594.

33. Michaud L, Beattie BJ, Akhurst T, Dunphy M, Zanzonico P, Finn R, et al. 18F-Fluciclovine (18F-FACBC) PET imaging of recurrent brain tumors. European Journal of Nuclear Medicine and Molecular Imaging 2020;47(6):1353-67.

34. Debus C, Afshar-Oromieh A, Floca R, Ingrisch M, Knoll M, Debus J, et al. Feasibility and robustness of dynamic 18F-FET PET based tracer kinetic models applied to patients with recurrent high-grade glioma prior to carbon ion irradiation. Scientific reports 2018;8(1):14760.

35. Shoup TM, Olson J, Hoffman JM, Votaw J, Eshima D, Eshima L, et al. Synthesis and evaluation of [18F]1-amino-3-fluorocyclobutane-1-carboxylic acid to image brain tumors. J Nucl Med 1999;40(2):331-8.

FIGURES

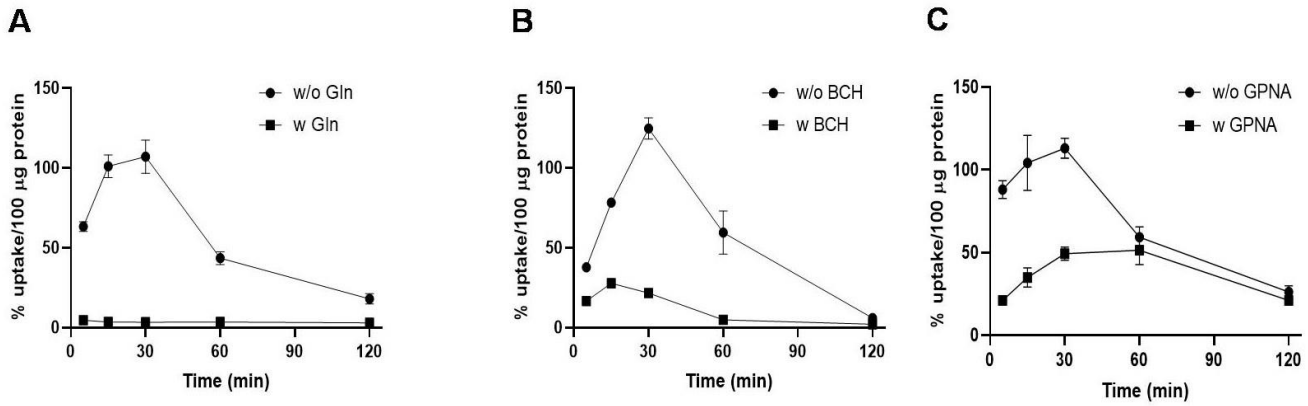

Figure 1: Cellular uptake of ^{18}F-Fluciclovine is mediated by glutamine transporters. Uptake into HCC1806 cells blocked by excess of glutamine (**A**), BCH (**B**) or GPNA (**C**). Glutamine (Gln, 5 mM), BCH (10 mM) or GPNA (1 mM) was added at time=0 to incubation media which was made of PBS containing 5 mM glucose (final concentration of these reagents are specified in parentheses). Each point in the graph represents the mean +/- stdev from four (4) replicates.

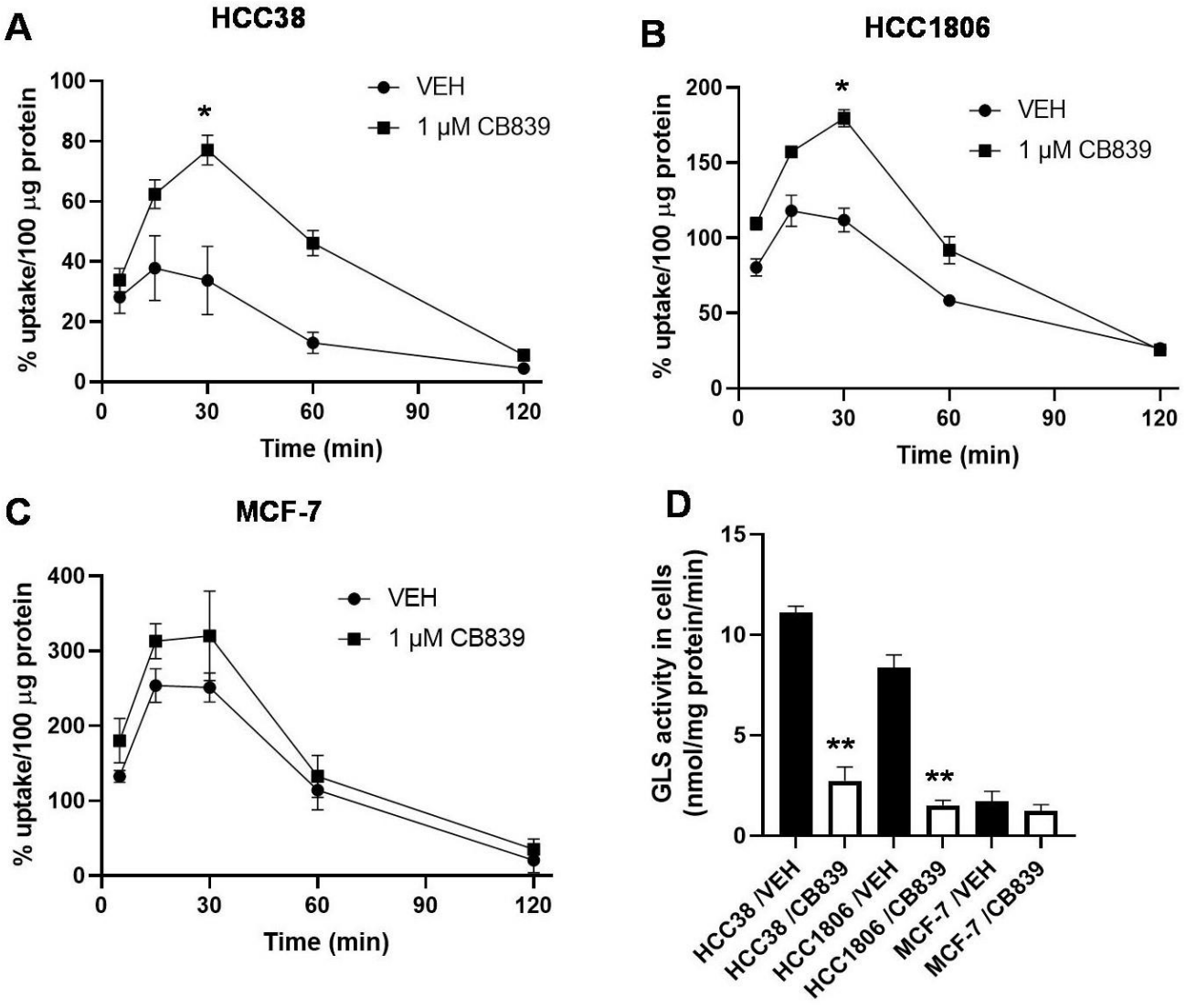

Figure 2: Cellular uptake of ^{18}F-Fluciclovine and GLS activity in TNBC and ER-positive breast cancer cells. Dynamic uptake profile of HCC38 (**A**), HCC1806 (**B**) and MCF-7 (**C**) cells, and *GLS* activities after CB839 or VEH treatment (**D**). Error bars are SD. *P* value comparing CB839 vs VEH group in (**D**): HCC38 /$4.58x10^{-5}$, HCC1806 /$7.12x10^{-5}$, MCF-7/ 0.22. (A-C): Each point in the graph represents the mean +/- stdev from four (4) replicates. D: Each bar represents the mean +/- stdev from three (3) mice.

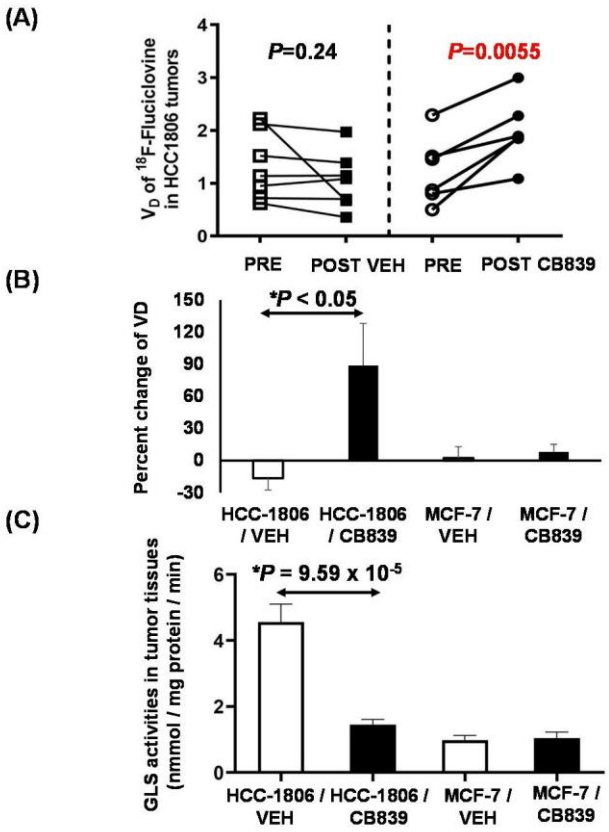

Figure 3: ^{18}F-Fluciclovine VD value before and after GLSi treatment and change of V_D induced by GLSi or VEH treatment and tumor GLS activities in TNBC and ER+ BC. (A) Pre and post-treatment V_D values of individual mice bearing HCC1806 tumor enrolled in VEH-treated (n=7) and CB839-treated group (n=6). Percent change of V_D (post/pre-1) of VEH treated and CB839 HCC1806 (n=7 / n=6 in VEH /CB839 group) and MCF-7 tumors (n=5 / n=4 in VEH /CB839 group) (**B**). GLS activities of VEH and CB839 treated HCC1806 and MCF-7 tumors (**C**) HCC1806 post CB839: 1.46 ± 0.13, n=4; HCC1806 post VEH: 4.56±0.44, n=3; MCF-7 post CB839: 1.07±0.17, n=5; MCF-7 post VEH: 0.99±0.12, n=3)**.**

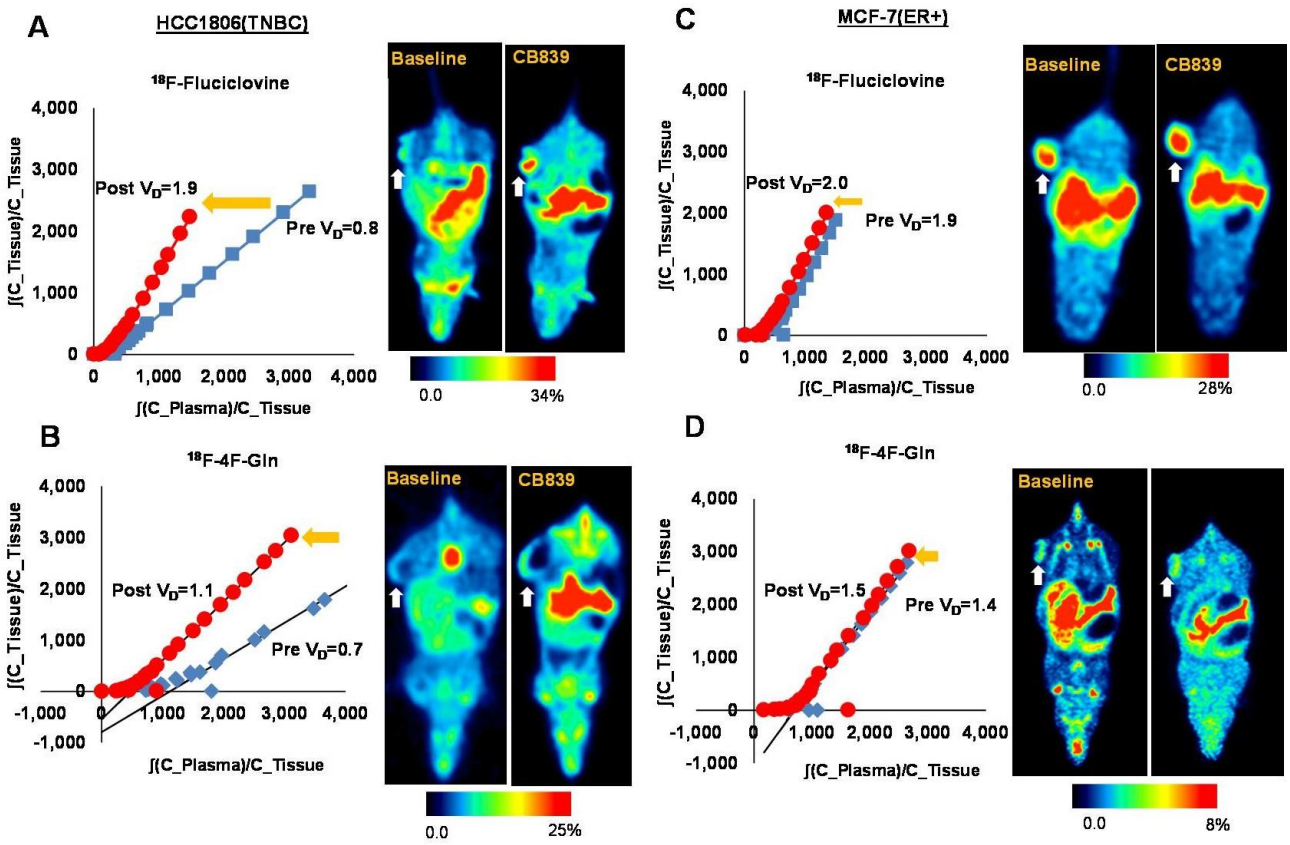

Figure 4: Comparison of ^{18}F-Fluciclovine *versus* ^{18}F-4F-Gln PET for detecting pharmacodynamic responses to GLSi. Logan plots and PET images of ^{18}F-Fluciclovine (**A**) versus ^{18}F-4F-Gln (**B**) at baseline and post CB839 treatment from representative mice bearing HCC1806 or MCF-7 tumors (**C**-**D**). Yellow arrows point to the tumor. Sample sizes for ^{18}F-4F-Gln study are reported earlier (Cancer Res 2017;77(6):1476-84) while those for ^{18}F-Fluciclovine are described in Figure 3. The same color scale (based on a percentage of maximum signal intensity) is applied to both pre- and post-treatment PET images.

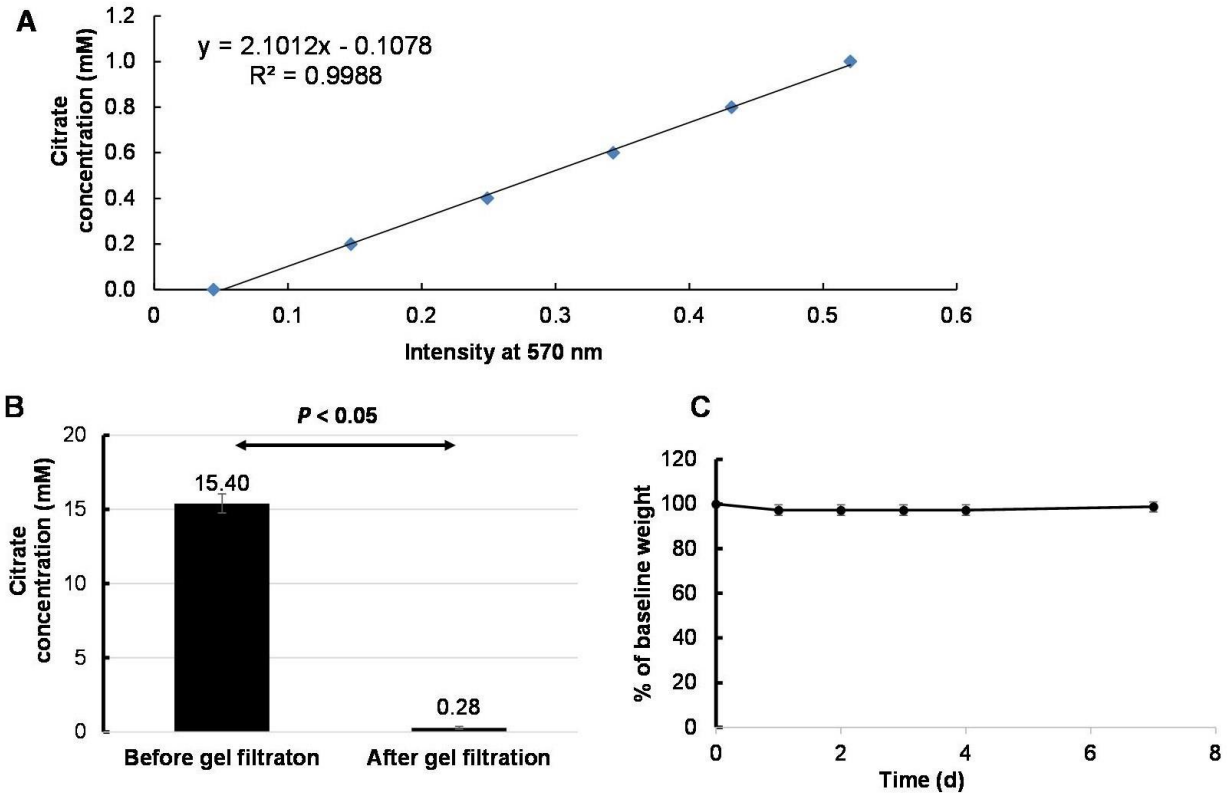

Supplemental Figure 1: Replacement of citrate in ^{18}F-Fluciclovine formulation with PBS. A: Standard curve of citrate assay. **B**: Citrate concentration before (n=2) and after filtration (n=3). *P* = 2.62×10^{-5}. **C**: Body weight of mice (n=3) after injection of filtered Fluciclovine solution (radioactivity was decayed).

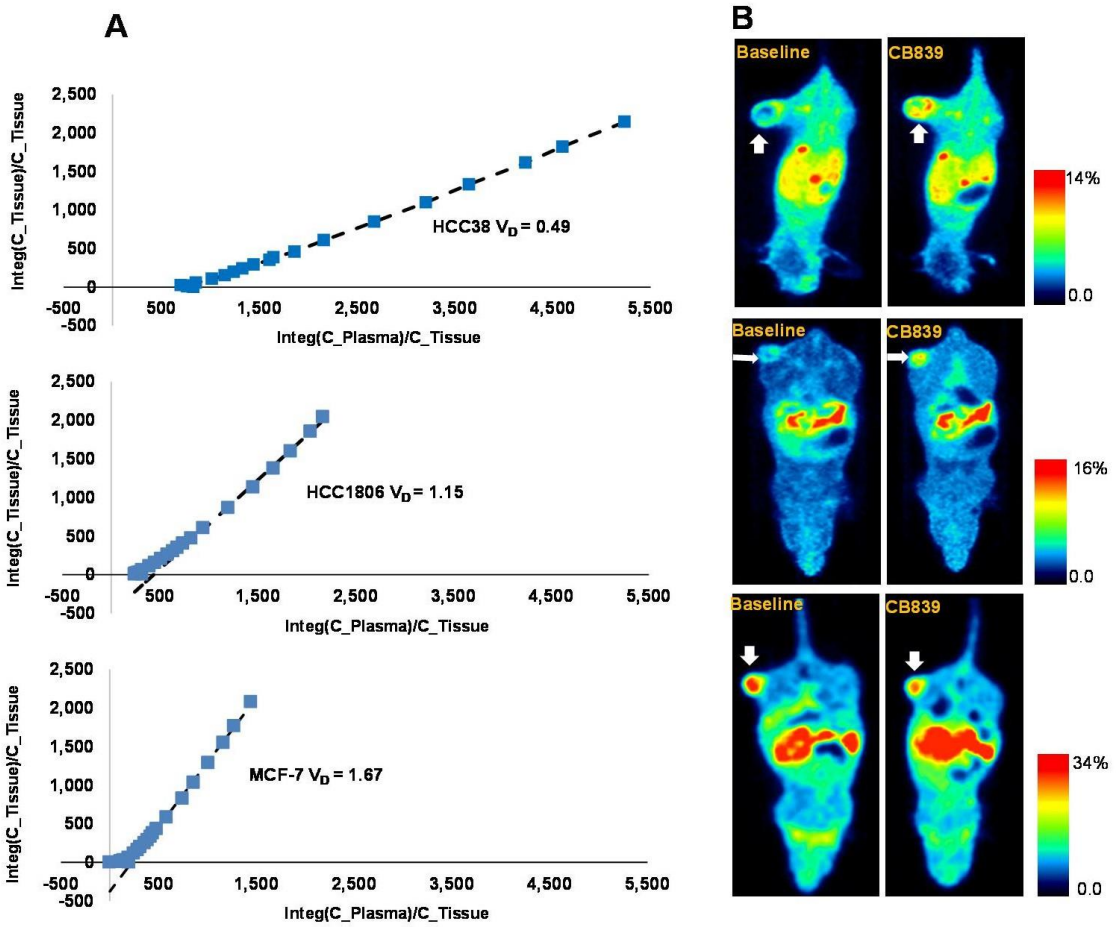

Supplemental Figure 2: ^{18}F-Fluciclovine PET images and Logan plots before and after GLSi treatment. A: Logan plots of TNBC (HCC38, HCC1806) and MCF-7 tumor at baseline. B: Pre- and post-CB839 treatment PET image of a representative mouse bearing HCC38, HCC1806 and MCF-7 tumor (from top to bottom). White arrows point to the tumor. The same color scale (based on a percentage of maximum signal intensity) is applied to both pre- and post-treatment PET images.

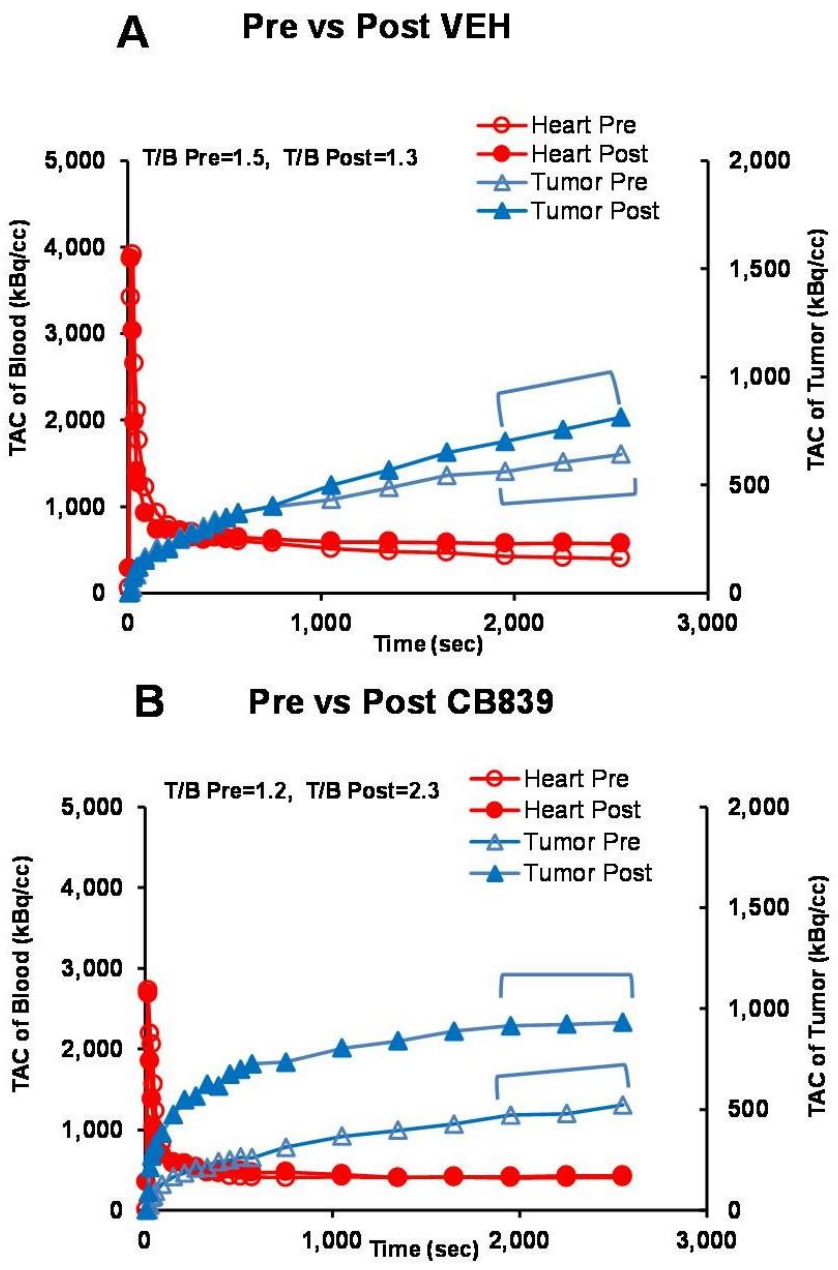

Supplemental Figure 3: Tumor uptake time course in a VEH (A) and CB839 treated mouse (B), respectively. TACs of tumor and blood were plotted together. The tumor-to-blood ratio (T/B) was obtained by averaging the intensity of the last three frames (15 min) of the tumor and blood TAC, respectively.

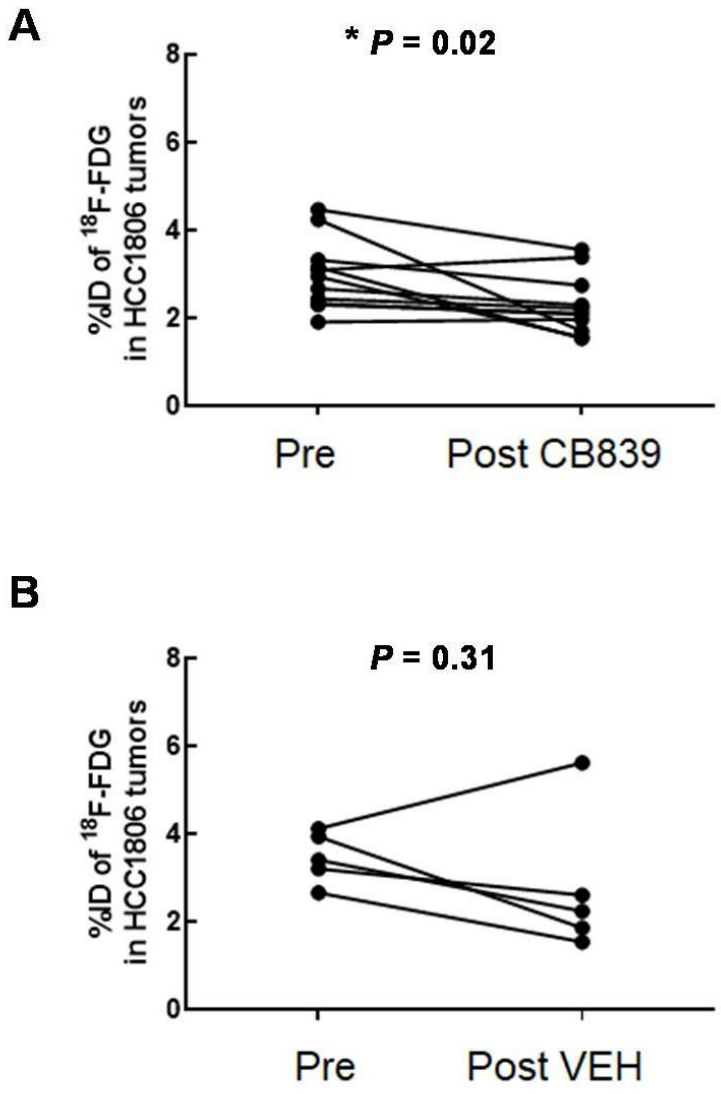

Supplemental Figure 4: Responses of FDG PET signals to GLSi treatment. %ID of FDG PET measured at pre and post CB839 (**A,** n=11) or VEH (**B,** n=5) treatment in HCC1806 tumors.

GRAPHICAL ABSTRACT